An Analytical Model for Line-Edge Roughness Limited Mobility of Graphene Nanoribbons

Arash Yazdanpanah Goharrizi, Mahdi Pourfath, *Member, IEEE*, Morteza Fathipour, *Member, IEEE*, Hans Kosina, *Member, IEEE*, and Siegfried Selberherr, *Fellow, IEEE*

***Abstract*—The electronic properties of graphene nanoribbons (GNRs) in the presence of line-edge roughness scattering are studied. The mobility, conductivity, mean free path, and localization length of carriers are analytically derived using an effective mass model for the band structure. This model provides a deep insight into the operation of armchair GNR devices in the presence of line-edge roughness. The effects of geometrical and roughness parameters on the electronic properties of GNRs are estimated assuming a diffusive transport regime. However, in the presence of disorder, localization of carriers can occur, which can significantly reduce the conductance of the device. The effect of localization on the conductance of rough nanoribbons and its dependences on the geometrical and roughness parameters are analytically studied. Since this regime is not suitable for the operation of electronic devices, one can employ these models to obtain critical geometrical parameters to suppress the localization of carriers in GNR devices.**

***Index Terms*—Diffusive transport, effective band gap, graphene, localization, mobility, quantum transport.**

I. Introduction

SINCE the miniaturization of silicon-based devices is approaching its limits, new transistor materials are desired [1]. For replacing silicon, many materials such as compound semiconductors, carbon nanotubes, and graphene have been studied. Graphene, which is a 2-D sheet of carbon atoms arranged in a honeycomb lattice, has been studied as a potential candidate for future electronic applications [2]–[6]. However, graphene is a gapless material. To induce an electronic band gap, graphene sheets are patterned into ribbons, which are so-called graphene nanoribbons (GNRs) [7]. GNRs are quasi-1-D materials with a band gap depending on the width of the ribbon and its crystallographic direction [8]. Experimental studies show that the mobility of GNRs is much lower than that of a graphene sheet [2], [9]. To improve the electronic properties of GNRs and to achieve a better insight into the operation of such devices, major sources of carrier scattering must be studied. For electronic applications, a band gap larger than 0.1 eV is essential. Therefore, the width of GNRs must be scaled below 10 nm to achieve this goal [8]. In narrow GNRs, edge disorders have a strong effect on the conductivity [10], [11]. Experimental data show that the line-edge roughness is the dominant scattering mechanism for GNRs of widths below 60 nm [12]. Line-edge roughness causes fluctuations in the edge potential and lead to the modulation of the band gap. Therefore, a comprehensive investigation of the effects of edge disorder is needed. The effect of edge disorder on the electronic properties of GNRs has been recently addressed in several numerical studies [13]–[20]. An analytical model for the localization length in GNR due to edge disorder has been presented in [21]. In that work, an Anderson model has been employed, and the correlation between edge disorders has been neglected. In this paper, however, we assume an exponential autocorrelation between edge disorders. Employing an effective mass model, analytical models for the mobility, conductivity, mean free path, and localization length for armchair GNRs have been derived. The conductance of GNRs is studied in both the diffusive transport and the localization regimes. The effect of localization is investigated by introducing an effective band gap, where analytical approximations for this quantity are presented. The effective mass is fitted to the tight binding band structure model, where up to three nearest neighbors and also the passivization of the dangling bonds with hydrogen are considered [22]. Employing this model, the effects of the width, temperature, and roughness parameters on the electronic properties of armchair GNRs are investigated. Comparison with numerical results shows the excellent accuracy of our analytical models. This paper is organized as follows: In Section II, the band structure model is discussed, and the quantities related to the band structure are derived. In Section III, the line-edge roughness model is discussed, followed by an analytical derivation of the mobility and conductivity in Section IV. The roles of the width, temperature, and roughness parameters are investigated in Section V. In Section VI, the localization of carriers in GNRs is discussed. Finally, concluding remarks are presented in Section VII.

Manuscript received February 11, 2011; revised April 21, 2011 and June 22, 2011; accepted July 27, 2011. Date of publication August 30, 2011; date of current version October 21, 2011. This work, as part of the European Science Fund, European Collaborative Research Program EuroGRAPHENE, was supported by Austrian Science Fund under Contract I420-N16. The review of this paper was arranged by Editor S. Deleonibus.

A. Y. Goharrizi and M. Pourfath are with the Department of Electrical and Computer Engineering, University of Tehran, Tehran, Iran, and also with the Institute for Microelectronics, Technische Universität Wien, 1040 Wien, Austria.

M. Fathipour is with the Department of Electrical and Computer Engineering, University of Tehran, Tehran, Iran.

H. Kosina and S. Selberherr are with the Institute for Microelectronics, Technische Universität Wien, 1040 Wien, Austria.

Color versions of one or more of the figures in this paper are available online at http://ieeexplore.ieee.org.

Digital Object Identifier 10.1109/TED.2011.2163719

II. Electronic Band Structure

It has been shown that a three nearest neighbor tight binding approximation along with an edge-distortion correction can

accurately predict the band structure of GNRs [22]. Using a Taylor expansion around the charge neutrality point, the band structure of an armchair GNR can be written as [22]

$$E_n^{\pm}(k_x) \approx \pm\sqrt{(E_{G,n}/2)^2 + (\hbar v_n)^2 k_x^2} \tag{1}$$

with

$$E_{G,n} \equiv 2\left[\gamma_1\left(2\cos(n\theta)+1\right) + \gamma_3\left(2\cos(2n\theta)+1\right) + \frac{4(\gamma_3+\Delta\gamma_1)}{N+1}\sin^2(n\theta)\right] \tag{2}$$

$$v_n^2 = \left(\frac{3a_{cc}}{\hbar}\right)^2 \times\left[-\frac{1}{2}\gamma_1\cos(n\theta) \times\left\{\gamma_1 + \gamma_3\left(2\cos(2n\theta)+1\right) + \frac{4(\gamma_3+\Delta\gamma_1)}{N+1}\sin^2(n\theta)\right\} - \gamma_3\left\{\gamma_1 + 2\gamma_3\cos(2n\theta) + \frac{4(\gamma_3+\Delta\gamma_1)}{N+1}\sin^2(n\theta)\right\}\right] \tag{3}$$

$$\theta = \frac{\pi}{N+1}. \tag{4}$$

In (1), $+$ and $-$ represent the conduction and the valence bands, respectively; N is the total number of A- and B-type carbon atoms in each chain of the ribbon (see Fig. 1); $n = 1, \ldots, N$ denotes the subband index; and $E_{G,n}$ and $E_{C,n}$ are the band gap and the band edge energy of the nth subband, respectively. Due to the symmetric band structure of electrons and holes, one obtains $E_{G,n} = 2E_{C,n}$. The first and third nearest neighbor hopping parameters are $\gamma_1 \approx -3.2$ eV and $\gamma_3 \approx -0.3$ eV, respectively. $\Delta\gamma_1 \approx -0.2$ eV is the correction to the first nearest neighbor due to edge distortion [22]. Using (2), one can straightforwardly show that the band gap of GNRs is inversely proportional to the ribbon's width [22], i.e.,

$$E_{G,n} \approx \frac{c}{W}. \tag{5}$$

For GNRs with indexes $N = 3p$, $N = 3p+1$, and $N = 3p+2$, where p is an integer, one can fit the band gap of the first subband to (5) with $c = 0.8$ eV $\cdot$ nm, $c = 1.6$ eV $\cdot$ nm, and $c = 0.4$ eV $\cdot$ nm, respectively (see Fig. 2).

A. Effective Mass Approximation

Applying a Taylor expansion to (1), the band structure of an armchair GNR can be approximated by an effective mass model as

$$E_n^{\pm}(k_x) \approx \pm\left(E_{C,n} + \frac{(\hbar v_n k_x)^2}{2E_{C,n}}\right) = \pm\left(E_{C,n} + \frac{\hbar^2 k_x^2}{2m_n^*}\right). \tag{6}$$

Effective mass m_n^* of subband n is given by

$$m_n^* = \frac{E_{C,n}}{v_n^2}. \tag{7}$$

The effective mass has width dependence through both terms in the numerator and the denominator, which are inversely

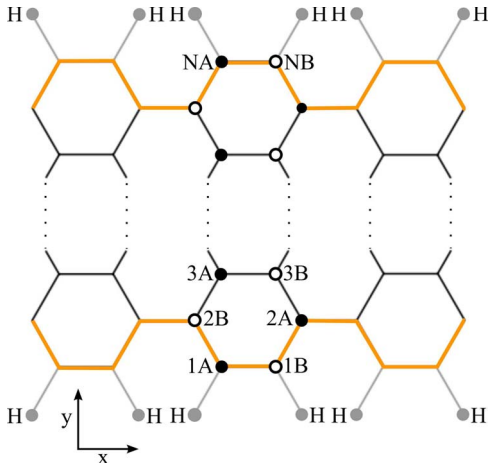

Fig. 1. Structure of a GNR with armchair edges and the x–y coordinate system. The edges of the GNR are terminated by hydrogen atoms.

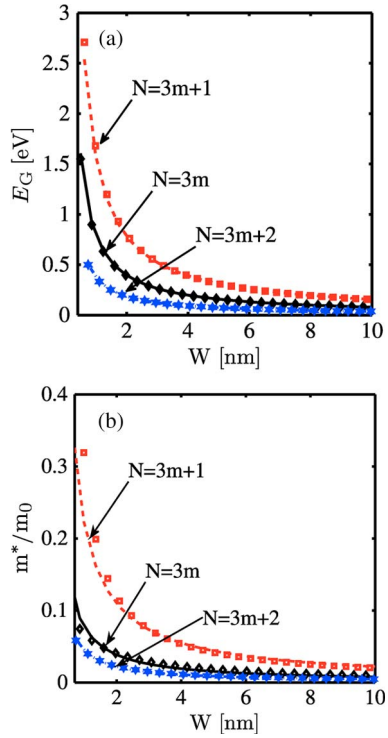

Fig. 2. (a) Band gap and (b) the effective mass of armchair GNRs as a function of the width for different GNR types. (Symbols) The exact values and (lines) the fitted curves.

proportional to the ribbon width. Therefore, the effective mass of the subbands can be approximated as

$$\frac{m_n^*}{m_0} \approx \frac{d}{W}. \tag{8}$$

For GNRs with indexes of $N = 3p$, $N = 3p+1$, and $N = 3p+2$, one can fit the effective mass of the first subband to (8) with $d = 0.7$ nm, $d = 2.0$ nm, and $d = 0.4$ nm, respectively (see Fig. 2).

B. Density of States and Carrier Concentration

Using the effective mass model, the density of states per unit length for the nth subband can be written as

$$\rho_n(E) = \frac{4}{2\pi}\left(\frac{\partial E}{\partial k}\right)^{-1} = \frac{\sqrt{2m_n^*}}{\pi\hbar}\frac{1}{\sqrt{E - E_{G,n}/2}}\Theta(E - E_{G,n}/2). \tag{9}$$

Here, Θ is the unit step function. The total density of states is given by $\rho(E) = \sum_n \rho_n(E)$. The electron concentration can be then evaluated as

$$n = \int_0^\infty \rho(E) f(E)\, dE. \tag{10}$$

We assume Fermi–Dirac distribution function $f(E) = 1/(1 + \exp[(E - E_F)/k_BT])$, where k_B is the Boltzmann constant, T is the temperature, and E_F is the Fermi level. The electron concentration follows from (10) as (see the Appendix)

$$n = \sqrt{\frac{2k_BT}{\pi\hbar^2}} \sum_n \sqrt{m_n^*} F_{-1/2}(\eta_n) \tag{11}$$

where $F_{-1/2}$ is the Fermi integral of order $-1/2$ [see (55)] and $\eta_n = (E_F - E_{G,n}/2)/k_BT$. In nondegenerate semiconductors, the Fermi integral can be approximated as $F_{-1/2}(\eta_n) \approx \exp(\eta_n)$, and the concentration can be thus approximated as

$$n \approx \sqrt{\frac{2k_BT}{\pi\hbar^2}} \sum_n \sqrt{m_n^*} \exp\left[\frac{(E_F - E_{G,n}/2)}{k_BT}\right]. \tag{12}$$

III. Line-Edge Roughness Scattering

Both experimental data [12] and theoretical predictions [10], [11], [13], [18] indicate that the line-edge roughness is the dominant source of scattering in narrow GNRs. Line-edge roughness is a statistical phenomenon that can be described by introducing an autocorrelation function [23]. An exponential autocorrelation is applied in this paper for evaluating transition matrix elements due to line-edge roughness. The scattering rate and the relaxation time are subsequently analytically derived.

A. Transition Matrix Elements

Using the Fermi-golden rule, the transition rate of electrons due to line-edge roughness from subband n with initial wave-vector k_x, represented by $|\psi_n(k_x)\rangle$, to another subband n' with final wave-vector k'_x, represented by $|\psi_{n'}(k'_x)\rangle$, can be written as

$$\mathcal{S}_{n,n'}(k_x, k'_x) = \frac{2\pi}{\hbar}\left|\langle\psi_{n'}(k'_x)|H_{\rm LER}|\psi_n(k_x)\rangle\right|^2 \times \delta\left(E_{n'}(k'_x) - E_n(k_x)\right). \tag{13}$$

The delta function states the energy conservation, where line-edge roughness scattering is assumed to be an elastic process. Due to open boundaries in the longitudinal direction (x-axis) and confinement along the transverse direction (y-axis), the electron wave functions are given by

$$\langle x|\psi_n(k_x)\rangle = \frac{1}{\sqrt{L}}\phi_n \exp(ik_x x). \tag{14}$$

Here, L is the length of the ribbon. In a ribbon with perfect edges, ϕ_n is only a function of transverse-direction $\phi_n = \phi_n(y)$. However, for ribbons with rough edges, ϕ_n also has some dependence on longitudinal direction $\phi_n = \phi_n(y, x)$. We assume smooth roughness, where one can neglect the dependence of ϕ_n on the longitudinal direction. Furthermore, ϕ_n is assumed to be normalized $\int_0^W |\phi_n(y)|^2 = 1$.

It is shown in Section II that the band edges and the electronic band gap of GNRs are inversely proportional to the ribbon's width $E_{G,n} = c/W$, where c is a constant. We assume that the band edges of the ribbon are modulated by the width fluctuations due to line-edge roughness. Therefore, the perturbation potential is given by [24]

$$H_{\rm LER}(x) = \delta E_{C,n} = -\frac{c}{W^2}\delta W = -\frac{\delta W(x)}{W}E_{C,n}. \tag{15}$$

$\delta W(x)$ denotes the width fluctuations, and $W = \langle W(x)\rangle$ is the average width of the ribbon as

$$\begin{aligned} M_{n,n'}(k_x, k'_x) &= \langle\psi_{n'}(k'_x)|H_{\rm LER}|\psi_n(k_x)\rangle \\ &= \frac{-E_{C,n}}{WL}\int_0^W \phi^*_{n'}(y)\phi_n(y)\, dy \int_0^L \delta W(x) \\ &\quad \times \exp\left[-i\left(k'_x - k_x\right)x\right] dx \\ &= \delta_{n,n'}\frac{-E_{C,n}}{WL}\int_0^L \delta W(x) \\ &\quad \times \exp\left[-i\left(k'_x - k_x\right)x\right] dx \end{aligned} \tag{16}$$

where only intrasubband transitions are considered ($n' = n$) [24]. Therefore, one can obtain the square of the transition matrix elements as

$$\left|M_n(k_x, k'_x)\right|^2 = \left(\frac{E_{C,n}}{WL}\right)^2 \int \delta W(x_1) \exp\left[+i\left(k'_x - k_x\right)x_1\right] \times dx_1 \int \delta W(x_2) \exp\left[-i\left(k'_x - k_x\right)x_2\right] dx_2. \tag{17}$$

The ensemble average of (17) leads to

$$\left|M_n(k_x, k'_x)\right|^2 = \left(\frac{E_{C,n}}{WL}\right)^2 \int\int \langle\delta W(x_1)\delta W(x_2)\rangle \times \exp\left[-iq.(x_1 - x_2)\right] dx_1\, dx_2. \tag{18}$$

Here, $q = k_x - k'_x$. The correlation between $\delta W(x_1)$ and $\delta W(x_2)$ can be described by an autocorrelation function as $R(x_1, x_2) = \langle \delta W(x_1) \delta W(x_2) \rangle$. For stationary processes, autocorrelation function $R(x_1, x_2)$ depends only on the relative distance between the points, i.e., $R(x_1, x_2) = R(x_1 - x_2)$. Therefore, one can introduce relative coordinate $x = x_1 - x_2$ and rewrite (18) as

$$|M_n(q)|^2 = \left(\frac{E_{C,n}}{WL}\right)^2 \int_0^L dx_1 \int R(x) \exp(-iqx)\, dx = \left(\frac{E_{C,n}}{W}\right)^2 \frac{G(q)}{L}. \tag{19}$$

The Fourier transform of autocorrelation function $G(q) = \int R(x) \exp(-iqx) dx$ is called the power spectral density. It is common to use a Gaussian or an exponential autocorrelation to describe line-edge roughness. In [23], an exponential autocorrelation function has been employed to model the Si/SiO_2 interface roughness. Furthermore, this autocorrelation function has been used in [24] to model line-edge roughness in GNRs. In this paper, we consider an exponential autocorrelation function to evaluate the transition matrix elements, i.e.,

$$R(x) = \Delta W^2 \exp\left(-\frac{|x|}{\Delta L}\right) \tag{20}$$

where ΔW is the root mean square of the fluctuation amplitude and ΔL is the roughness correlation, which is a measure of smoothness. The power spectrum of $R(x)$ is obtained as

$$G(q) = \frac{\Delta W^2 \Delta L}{1 + q^2 \Delta L^2}. \tag{21}$$

Using (19) and (21), the transition rate [see (13)] can be evaluated as

$$\mathcal{S}_n(k_x, k'_x) = \frac{4\pi}{\hbar} \frac{E_{C,n}^2}{W^2 L} \frac{\Delta W^2 \Delta L}{1 + q^2 \Delta L^2} \delta\left(E_{n'}(k'_x) - E_n(k_x)\right). \tag{22}$$

We assume two rough edges for the ribbon. Under the condition that the roughness of these two edges are uncorrelated, one can simply multiply the transition rate by a factor of two [see (22)].

B. Relaxation Time

To obtain the conductivity and the mobility of GNRs, the relaxation time due to line-edge roughness must be evaluated. Using (22), the relaxation time for electrons at some subband n with wave-vector k_x is given by

$$\frac{1}{\tau_n(k_x)} = \sum_{k'_x} \mathcal{S}_n(k_x, k'_x) \left(1 - \frac{|k'_x|}{|k_x|} \cos\alpha\right) \left(1 - f(k'_x)\right) \approx \frac{L}{\pi} \int \frac{4\pi}{\hbar} \frac{E_{C,n}^2}{W^2 L} \frac{\Delta W^2 \Delta L}{1 + q^2 \Delta L^2} \left(1 - \frac{|k'_x|}{|k_x|} \cos\alpha\right) \times \delta\left(E_{n'}(k'_x) - E_n(k_x)\right) dk'_x \tag{23}$$

where the summation runs over all final states k'_x and α is the angle between the initial and final wave vectors. GNRs are quasi-1-D and carriers that can be only backscattered, i.e., $\alpha = \pi$. Furthermore, we assume that line-edge roughness induces only intrasubband transitions. Therefore, $k'_x = -k_x$ or equivalently $q = k_x - k'_x = 2k_x$. In nondegenerate semiconductors, the probability of finding the final state empty is very high. It is, therefore, reasonable to use approximation $(1 - f(k'_x)) \approx 1$, which significantly simplifies the derivation of the relaxation time. By converting the integral over wave vector into energy and using (6), the relaxation time is obtained as

$$\frac{1}{\tau_n(E)} = \left(\frac{\Delta W}{W}\right)^2 \frac{4 m_n^* E_{G,n}^2 \Delta L}{\hbar^3} \int \frac{\delta\left(k_x'^2 - k_x^2\right)}{1 + (k_x - k'_x)^2 \Delta L^2} dk'_x = \left(\frac{\Delta W}{W}\right)^2 \frac{4 m_n^* E_{G,n}^2 \Delta L}{\hbar^3 k_x \left(1 + 4 k_x^2 \Delta L^2\right)}. \tag{24}$$

Using relation $k_x = \sqrt{(2m_n^*/\hbar^2)(E - E_{G,n}/2)}$, the relaxation time for electrons at subband n due to line-edge roughness scattering can be written as

$$\tau_n(E) = \left(\frac{W}{\Delta W}\right)^2 \times \frac{\hbar^2 \left(1 + 8 m_n^* (E - E_{G,n}/2) \Delta L^2/\hbar^2\right) \sqrt{E - E_{G,n}/2}}{2\sqrt{2 m_n^*} E_{G,n}^2 \Delta L}. \tag{25}$$

IV. Electronic Properties

Using the analytical models derived in Sections II and III, the conductivity and the mobility of GNRs in the presence of line-edge roughness are evaluated here.

A. Conductivity

In the framework of the linear response theory, the conductivity in some subband n can be written in the following form:

$$\sigma_n = \frac{q^2}{\pi\hbar} \int_0^\infty v_{g,n} \tau_n(E) (-\partial f/\partial E)\, dE \tag{26}$$

where $v_{g,n} = \hbar^{-1} \partial E/\partial k = \sqrt{2(E - E_{C,n})/m_n^*}$ is the group velocity of the respective subband, τ_n is the relaxation time, and f is the Fermi–Dirac distribution function. Using (25), the conductivity can be expressed as

$$\sigma_n = \left(\frac{W}{\Delta W}\right)^2 \frac{q^2 \hbar}{2\pi m_n^* E_{G,n}^2 \Delta L k_B T} \times \Bigg[\underbrace{\int_0^\infty \frac{(E - E_{C,n}) \exp[(E - E_F)/k_B T]}{\left(1 + \exp[(E - E_F)/k_B T]\right)^2} dE}_{A} + \frac{8 \Delta L^2 m_n^*}{\hbar^2} \times \underbrace{\int_0^\infty \frac{(E - E_{C,n})^2 \exp\left[(E - E_F)/k_B T\right]}{\left(1 + \exp\left[(E - E_F)/k_B T\right]\right)^2} dE}_{B} \Bigg]. \tag{27}$$

Assuming that the GNR is nondegenerately doped, one can approximate the Fermi–Dirac distribution function with

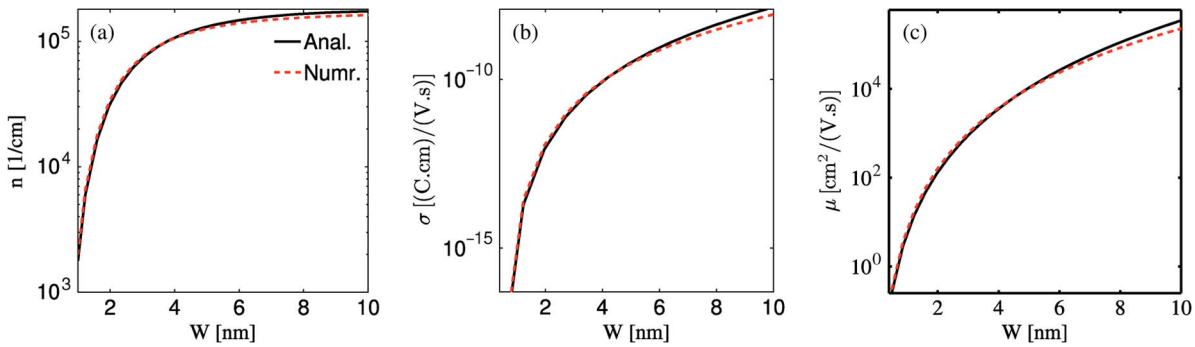

Fig. 3. Comparison between the numerical results and the analytical models of the (a) carrier mobility, (b) conductivity, and (c) concentration as a function of the GNR width for $E_F = 0.6E_C$, $\Delta W = 0.5$ nm, $\Delta L = 3$ nm, and $T = 300$ K. (Dashed curves) The numerical results and (solid lines) the analytical models.

$\exp[(E_F - E)/k_BT]$. Therefore, the two integrals in (27) can be approximated as

$$A = (k_BT)^2 \exp\left[-(E_{G,n}/2 - E_F)/k_BT\right] \tag{28}$$

$$B = 2(k_BT)^3 \exp\left[-(E_{G,n}/2 - E_F)/k_BT\right]. \tag{29}$$

Finally, the conductivity due to each subband of a GNR can be obtained as

$$\sigma_n = \left(\frac{W}{\Delta W}\right)^2 \frac{q^2\hbar k_BT}{2\pi m_n^* E_{G,n}^2 \Delta L}\left[1 + \frac{16\Delta L^2 m_n^*}{\hbar^2}k_BT\right] \times \exp\left[(E_F - E_{G,n}/2)/k_BT\right]. \tag{30}$$

B. Mobility

The mobility is given by $\mu = \sigma/(qn)$, where σ is the total conductivity and n is the carrier concentration due to all the subbands. However, in a nondegenerate case, it is reasonable to assume that the first subband mostly contributes to the total mobility and approximate it with $\mu \approx \sigma_1/(qn_1)$. Under this assumption and using (12) and (30), the mobility can be approximated as

$$\mu = \left(\frac{W}{\Delta W}\right)^2 \frac{q\hbar^2\sqrt{k_BT}}{2\sqrt{2\pi m_1^{*3}} E_{G,1}^2 \Delta L}\left(1 + \frac{16\Delta L^2 m_1^*}{\hbar^2}k_BT\right). \tag{31}$$

V. Analysis of Rough GNRs in Diffusive Transport Regime

Here, the influence of geometrical and roughness parameters on the electronic properties of armchair GNRs are investigated. We consider $N = 3p + 1$ type of GNRs. Here, analytical results are compared with numerical results, where only the first subband is considered without any parabolic approximation. For comparison with the experimental data along with the analytical model, full band calculations are also performed. In numerical calculations, the carrier concentration, scattering rate, and conductivity are evaluated according to (10), (22), and (26), respectively.

A. Ribbon Width

To make a comparison between the derived analytical formulas and the numerical results, mobility, conductivity, and electron concentration are evaluated as a function of the ribbon's width. We assume $E_F = 0.6E_C$ for all results. The numerical results are based on full band calculations with parameters described in Section II. As shown in Fig. 3, there is an excellent agreement between the analytical model and the numerical calculations. The discrepancy between the analytical model and numerical calculations appears at wide ribbons, where the energy band gap of the first subband becomes very close to the Dirac point. Under this condition, the nondegenerate assumption will not be accurate.

The electron concentration depends on the width of the ribbon through the effective mass and the exponential term in (12). The effective mass is inversely proportional to the ribbon's width [see (8)]. Letting $E_F \propto E_G$ and $E_G \propto W^{-1}$ [see (5)], the exponential term in (12) is proportional to $\exp(-p/W)$, where p is a constant, i.e.,

$$n \propto W^{-1/2}\exp(-p/W). \tag{32}$$

Equation (30) indicates that the conductivity of GNRs contains two parts. As the effective mass and the band gap are inversely proportional to the width of the ribbons, the first term of the conductivity is proportional to W^5 and the second term to W^4, i.e.,

$$\sigma \propto W^5(1 + \alpha/W)\exp(-p/W) = \begin{cases} W^5\exp(-p/W) & \alpha/W \ll 1 \\ \alpha W^4\exp(-p/W) & \alpha/W \gg 1 \\ (W^5 + \alpha W^4)\exp(-p/W) & \text{otherwise} \end{cases} \tag{33}$$

where $\alpha/W = 16m_n^*\Delta L^2 k_BT/\hbar^2$, and by using (8), one obtains $\alpha = 16m_0 d\Delta L^2 k_BT/\hbar^2$.

It can be easily shown that the first term in the mobility is proportional to $W^{5.5}$ and the second term to $W^{4.5}$ as

$$\mu \propto W^{5.5}(1 + \alpha/W) = \begin{cases} W^{5.5} & \alpha/W \ll 1 \\ \alpha W^{4.5} & \alpha/W \gg 1 \\ (W^{5.5} + \alpha W^{4.5}) & \text{otherwise.} \end{cases} \tag{34}$$

Under the condition of scaling with constant carrier concentration, the mobility, however, scales with $W^5 + \alpha W^4$. The

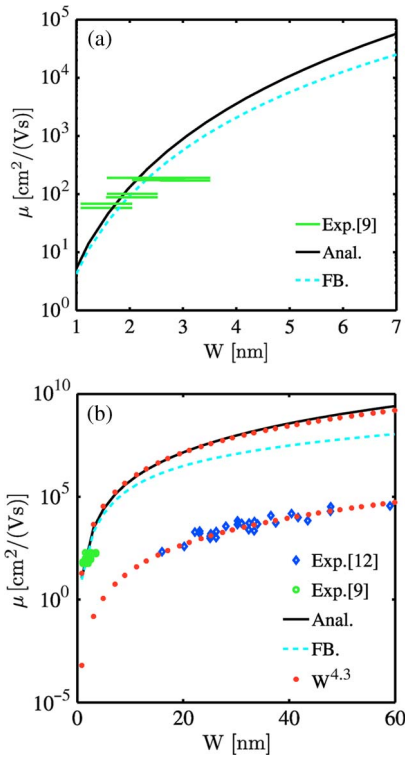

Fig. 4. Comparison between the experimental data and analytical model of the carrier mobility for $T = 300$ K and $\Delta W = 0.5$ nm. (a) $\Delta L = 3$ nm. (b) $\Delta L = 15$ nm.

mobility obtained from our analytical model is compared with the experimental data of [9] for $W < 4$ nm [see Fig. 4(a)] and [12] for $20 < W < 60$ nm (see Fig. 4). Roughness parameters have not reported in the experimental data; however, we assumed a roughness amplitude of 0.5 nm for both data and roughness correlation lengths of 3 and 15 nm to fit our model to the data shown in Fig. 4(a) and (b), respectively.

Reference [12] shows that the mobility of GNRs scales with the width as AW^B, where A is a constant and $B = 4.3$. In agreement with the experimental data, our analytical model also predicts a $A \cdot W^{4.3}$ trend for the mobility (see Fig. 4). However, the results are different within constant A, which is independent of the width. We believe this difference is due to the presence of other width independent scattering mechanisms such as phonon scattering and Coulomb scattering due to impurities at the graphene–substrate interface. It should be noted that if the experimental data of [9] is extrapolated to wider ribbons, much larger mobility will be obtained as compared with those given in [12]. This can be due to a better structural quality of ribbons obtained by chemical methods [12]. As the width of the ribbon increases, the energy difference between subband becomes smaller than k_BT. Under this condition, the contribution of higher subbands cannot be neglected. The evaluated mobility employing a full band calculation, where all subbands are included and nonparabolic dispersions are assumed, are shown in Fig. 4. Apparently, the effective mobility obtained from the full band calculations is lower than that predicted by a single-band effective mass model. This can be attributed to larger effective masses or lower mobility of higher subbands.

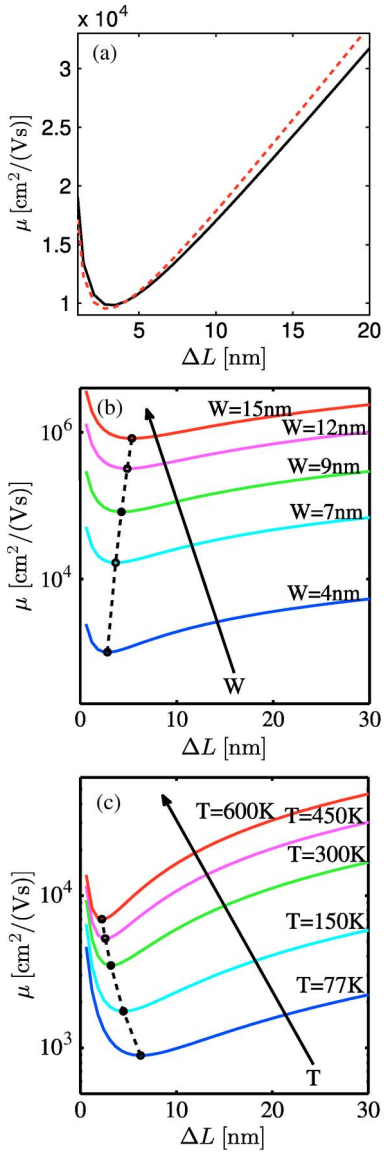

Fig. 5. (a) Comparison between the numerical results and the analytical models of the carrier mobility as a function of the roughness correlation length. (Dashed curves) The numerical results and (solid curves) the analytical models for $W = 5$ nm, $\Delta W = 0.5$ nm, and $T = 300$ K. (b) The carrier mobility as a function of the correlation length for various GNR widths at $\Delta W = 1$ nm and $T = 300$ K. (c) The carrier mobility as a function of the correlation length at various temperatures for $W = 5$ nm and $\Delta W = 1$ nm. $E_F = 0.6E_C$ for all figures.

B. Roughness Parameters

Fig. 5(a) compares the analytically and numerically evaluated mobility as a function of the roughness correlation length. As shown in Fig. 5, one can define critical correlation length ΔL_C, where the mobility and the conductivity reach their minimum values. Using (31), the critical correlation length can be obtained as

$$\Delta L_C = \frac{h}{8\pi\sqrt{m^* k_B T}}. \tag{35}$$

At ΔL_C, the roughness correlation length becomes comparable the de Broglie wavelength of thermal electrons, and the scattering rate will be maximum at this point [see (31)]. Therefore,

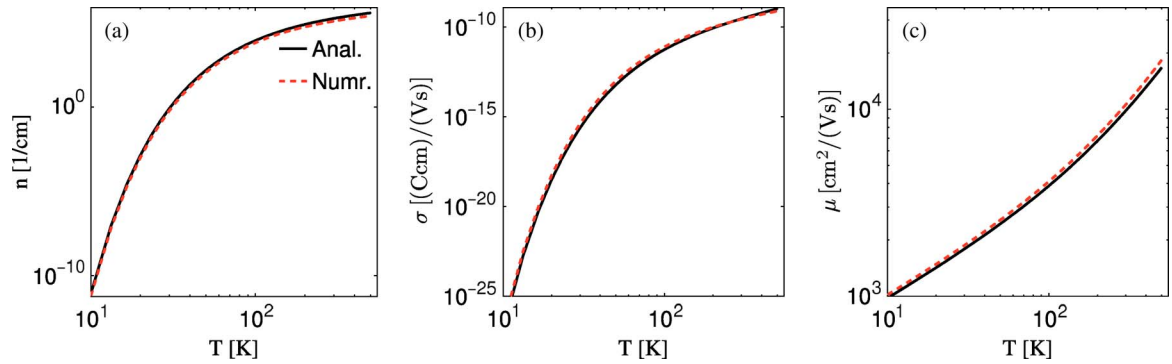

Fig. 6. Comparison between the numerical results and the analytical models of the (a) carrier mobility, (b) conductivity, and (c) concentration as a function of temperature for $W = 2$ nm, $E_F = 0.5E_C$, $\Delta L = 3$ nm, and $\Delta W = 0.5$ nm.

both the conductivity and the mobility take a minimum at this critical correlation length. As the width increases, the effective carrier mass decreases, and the minimum of mobility thus occurs at larger correlation lengths [see Fig. 5(b)]. As the temperature increases, the average kinetic energy of carriers increases, which results in the reduction of the thermal de Broglie wavelength. Therefore, the minimum occurs at shorter correlation lengths [see Fig. 5(c)].

C. Role of Temperature

Fig. 6 compares the carrier concentration, conductivity, and mobility obtained from the analytical formula and the numerical results. Using (12), (30), and (31), the temperature dependence of the carrier concentration, conductivity, and mobility can be written as

$$n \propto T^{1/2}\exp(-q/T) \tag{36}$$

$$\sigma \propto T(1+\beta T)\exp(-q/T) = \begin{cases} \beta T^2\exp(-q/T) & \beta T \gg 1 \\ T\exp(-q/T) & \beta T \ll 1 \\ (T+\beta T^2)\exp(-q/T) & \text{otherwise} \end{cases} \tag{37}$$

$$\mu \propto T^{1/2}(1+\beta T) = \begin{cases} \beta T^{3/2} & \beta T \gg 1 \\ T^{1/2} & \beta T \ll 1 \\ (T^{1/2}+\beta T^{3/2}) & \text{otherwise} \end{cases} \tag{38}$$

where $q = (E_{C,n} - E_F)/k_B$ and $\beta = 16m_n^*\Delta L^2 k_B/\hbar^2$.

VI. Localization of Carriers

In the absence of scattering, carrier transport is in the ballistic regime. In this regime, the conductance is independent of the device length. In the presence of scattering, transport of carriers is in the diffusive regime, where the spectrum of conductance is inversely proportional to device length(L), i.e.,

$$G(E) \approx G_0 \frac{1}{1+L/\lambda(E)}\left(-\frac{\partial f}{\partial E}\right) \tag{39}$$

with $G_0 = 2q^2/h$. In this regime, the mean free path of carriers can be defined as $\lambda(E) = v_g(E)\tau(E)$. However, in the presence of a disorder, the carrier wave packet can be scattered back and forth between potential barriers and standing waves along the device can develop. In this regime, referred to as localization regime, the transport of carriers takes place by tunneling between localized states, and the spectrum of conductance of the ribbon exponentially decreases with the ribbon's length [25] as

$$G(E) \approx G_0 \exp\left[-\frac{L}{\xi(E)}\right]\left(-\frac{\partial f}{\partial E}\right). \tag{40}$$

It should be noted that (40) is valid as long as the coherence length of electrons is longer than the device length. Phase breaking scattering mechanisms such as phonon scattering can reduce the coherence length. Experimental results show that graphene has high electron mobility at room temperature, with reported values in excess of 15 000 $\text{cm}^2/(\text{V}\cdot\text{s})$ [3]. Scattering by the acoustic phonons of graphene places intrinsic limits on the room temperature mobility to 200 000 $\text{cm}^2/(\text{V}\cdot\text{s})$ [26], [27]. However, for graphene on SiO_2 substrates, scattering of electrons by optical phonons of the substrate is a larger effect at room temperature than scattering by graphene's own optical phonons. This limits the mobility to 40 000 $\text{cm}^2/(\text{V}\cdot\text{s})$ [26]. As a result, a relatively large coherence length in graphene-based structures is observed [28], [29]. It has been experimentally shown that strong localization can appear in single-layer GNRs [30] and nanotubes at room temperature [31].

It has been shown that the localization length in quasi-1-D devices is related to the mean free path by [32] $\xi_n(E) \approx N_{\text{ch}}(E)\lambda_n$, where $N_{\text{ch}}(E)$ denotes the number of active conducting channels at some energy E.

A. Localization Length and Mean Free Path

Using (25) and replacing $v_{g,n}$, the mean free path due to line-edge roughness scattering can be obtained as

$$\lambda_n(E) = v_{g,n}(E)\tau_n(E) = \left(\frac{W}{\Delta W}\right)^2 \times \frac{\hbar^2\left(1+8m_n^*(E-E_{G,n}/2)\Delta L^2/\hbar^2\right)(E-E_{G,n}/2)}{2m_n^*\Delta L E_{G,n}^2} = C\left\{(E-E_{G,n}/2)+D(E-E_{G,n}/2)^2\right\} \tag{41}$$

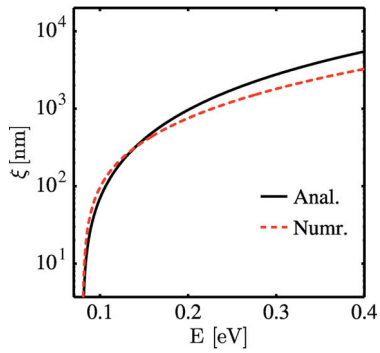

Fig. 7. Comparison between the numerical results and the analytical models for the localization length as a function of energy for $E_F = 0.6E_C$, $\Delta L = 3$ nm, $\Delta W = 0.3$ nm, $W = 5$ nm, and $T = 300$ K. (Dashed curves) The numerical results and (solid curves) the analytical models.

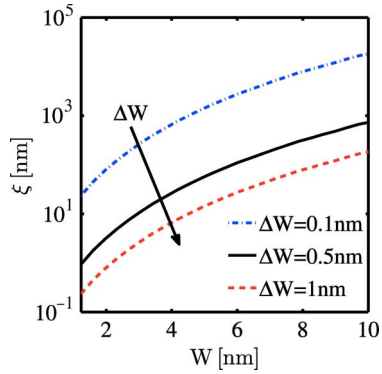

Fig. 8. Localization length as a function of the GNR width for different roughness amplitudes ΔW for $\Delta L = 3$ nm, $E_F = 0.6E_C$, $E = 1.2E_C$ and $T = 300$ K.

with

$$C = \left(\frac{W}{\Delta W}\right)^2 \frac{\hbar^2}{2m_n^* \Delta L E_{G,n}^2} \tag{42}$$

$$D = \frac{8m_n^* \Delta L^2}{\hbar^2}. \tag{43}$$

In a nondegenerate device with large splitting of the subbands, the first subband mostly contributes to the total carrier transport, i.e., $N_{\text{ch}} = 1$. In this case, one can approximate the localization length as $\xi(E) \approx \lambda(E)$. As shown in Fig. 7, the localization length is very small for carriers close to the conduction band and increases as the kinetic energy of the carrier increases. The width dependence of the mean free path and the localization length for energies close to the subband edges can be given by

$$\lambda = \xi \propto W^4(1 + \gamma/W^2) = \begin{cases} \gamma W^2 & \gamma/W^2 \gg 1 \\ W^4 & \gamma/W^2 \ll 1 \\ (W^4 + \gamma W^2) & \text{otherwise} \end{cases} \tag{44}$$

with $\gamma/W^2 = 8c\Delta L^2/\hbar^2$. If the ribbon has large effective mass (narrow GNRs) or large correlation length, the localization length and the mean free path scale as $\lambda, \xi \propto W^2$ (see Fig. 8).

B. Conductance in the Localization Regime

Fig. 9 compares the conductance of GNRs in the diffusive and localization regime. Fig. 9(a) indicates that, at the same width, localization of carriers is more pronounced in longer GNRs. Fig. 9(b) shows that, at the same length, localization is more pronounced in narrower GNRs. This behavior can be well understood by considering the energy dependence of the conductance spectrum at different lengths (see Fig. 10). For energies above the conduction band edge, the exponential tail of the Fermi function decreases, whereas term $\exp[-L/\xi(E)]$ increases due to the increase in the localization length [see Fig. 7]. As a result, the conductance spectrum peaks at some energy $E_{\max}$. One can define this energy as an effective band edge for carriers. In a similar way, an effective band gap can be also defined. In the following, analytical solutions for the

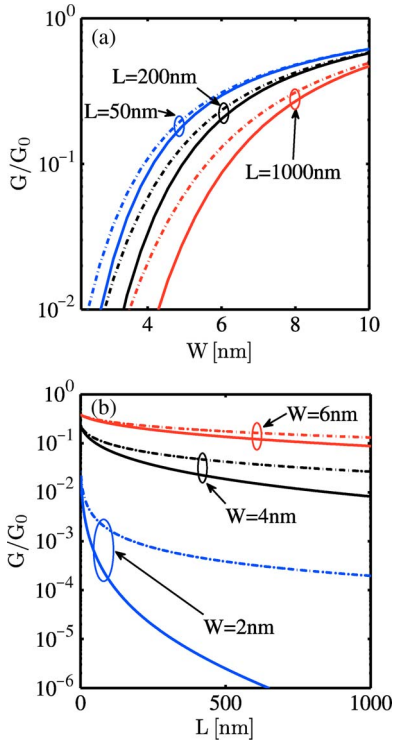

Fig. 9. Comparison of conductance in the (solid curves) localization and (dash-dot curves) diffusive regime (a) as a function of the width and (b) as a function of the length. $\Delta W = 0.5$ nm, $\Delta L = 3$ nm, $E_F = 0.6E_C$, and $T = 300$ K.

effective band edge and band gap are derived. The peak of the conductivity occurs at

$$\frac{\partial \xi(E)}{\partial E} = \frac{1}{k_B T L}\xi^2(E). \tag{45}$$

By substituting $\xi(E)$ from (41), a quadratic equation is obtained for the difference between the effective band gap and band structure gap $\Delta E_G = 2(E_{\max} - E_{G,n}/2) = E_{\text{Geff}} - E_G$ as

$$\left(\frac{\Delta E_G}{2}\right)^4 + \frac{2}{D}\left(\frac{\Delta E_G}{2}\right)^3 + \frac{1}{D^2}\left(\frac{\Delta E_G}{2}\right)^2 - \frac{2k_B T L}{CD}\left(\frac{\Delta E_G}{2}\right) - \frac{k_B T L}{CD^2} = 0. \tag{46}$$

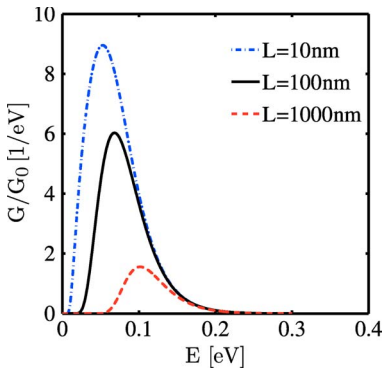

Fig. 10. Spectrum of conductance in the localization regime as a function of energy for different GNR lengths L and $\Delta W = 0.5$ nm, $\Delta L = 3$ nm, $W = 5$ nm, $E_F = 0.6E_C$, and $T = 300$ K.

ΔE_G can be evaluated by solving (46) as follows:

$$\Delta E_G = \left[Z^{1/2} + \left(\frac{4k_BTL}{CDZ^{1/2}} - Z' \right)^{1/2} - \frac{1}{D} \right] \tag{47}$$

with

$$Z = 2Y - \frac{1}{2D^2} \tag{48}$$

$$Z' = 2Y - \frac{3}{2D^2} \tag{49}$$

$$Y = \begin{cases} \frac{5}{12D^2} + \left(\frac{1}{2^2 3^3 D^6} + \frac{(k_BTL)^2}{2C^2D^2} \right)^{1/3} & U = 0 \\ \frac{5}{12D^2} + U + \frac{1}{2^3 3^2 D^4 U} & U \neq 0. \end{cases} \tag{50}$$

U is defined as

$$U = \left[\left(\frac{1}{6D^2} \right)^3 + \left(\frac{k_BTL}{2CD} \right)^2 + \left(\frac{7}{2^9 3^6 D^{12}} + \left(\frac{k_BTL}{2CD} \right)^4 + \frac{(k_BTL)^2}{2^4 3^3 C^2 D^8} \right)^{1/2} \right]^{1/3}. \tag{51}$$

Equation (47) gives the exact solution for ΔE_G.

However, for $D \ll 1/(E - E_{G,n}/2)$ and $D \gg 1/(E - E_{G,n}/2)$, the localization length can be approximated as $\xi(E) = C(E - E_{G,n}/2)$ and $\xi(E) = CD(E - E_{G,n}/2)^2$, respectively. Therefore, ΔE_G is given by

$$\Delta E_G = \begin{cases} 2\left(\frac{k_BTL}{C}\right)^{1/2} & D \ll \left(\frac{C}{k_BTL}\right)^{1/2} \\ 2\left(\frac{2k_BTL}{CD}\right)^{1/3} & D \gg \left(\frac{C}{2k_BTL}\right)^{1/2}. \end{cases} \tag{52}$$

The validity of this approximation is investigated for different geometrical and roughness parameters in Fig. 11. As length L or roughness amplitude increases, the effective band gap increases and the conductance is significantly reduced. With the increase in the width, however, the effective band gap is reduced. Fig. 11(d) shows the effective band gap as a function of the correlation length. The effective band gap has a maximum at some correlation length. As the width of the ribbon increases, this peak occurs at longer correlation lengths. With the presented relation, one can obtain the window of geometrical parameters where localization of carriers is avoided. On the other hand, for the given geometrical and roughness parameters, one can evaluate the effective band gap and the resulting reduction of the conductivity. Assuming exponential dependence of the current on the band gap, one can roughly estimate the changes of the current due to the presence of localization by $\Delta I \propto \exp(-\Delta E_G/k_BT)$.

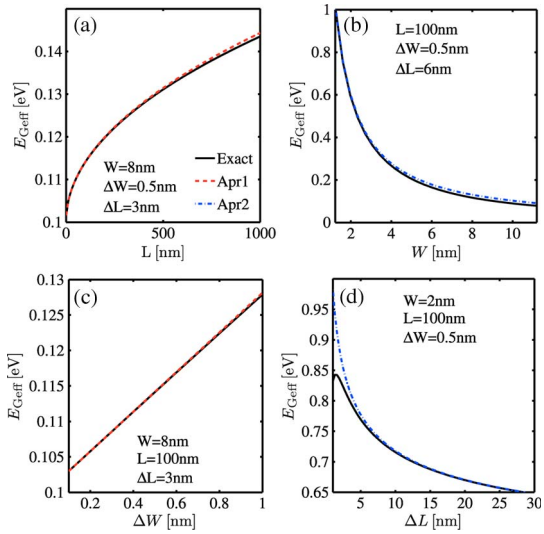

Fig. 11. Comparison between the exact effective band gap and the two approximations as a function of geometrical and roughness parameters. $E_F = 0.6E_C$, and $T = 300$ K.

VII. Conclusion

GNRs with band gaps suitable for electronic applications have a width below 10 nm. In this regime, line-edge roughness is the dominant scattering mechanism. Under this condition, analytical models for the mobility, conductivity, concentration, mean free path, and localization length of carrier in GNRs are derived. Using these analytical models, the dependences of the mentioned quantities on the geometrical and roughness parameters have been studied and discussed. Our predicted width dependence of the mobility is in excellent agreement with the experimental data. The role of carrier localization on the conductance of rough nanoribbons has been studied, and the related analytical models have been derived. Employing these models, one can appropriately select the geometrical parameters for optimizing the performance of GNR-based electronic devices.

Appendix

By substituting (9) in (10), the carrier concentration can be written as

$$n = \int_0^\infty \sum_n \rho_n(E) f(E)\, dE = \sum_n \frac{\sqrt{2m_n^*}}{\pi\hbar} \int_0^\infty \frac{\Theta(E - E_{G,n}/2)}{\sqrt{(E - E_{G,n}/2)}} \frac{dE}{1 + \exp\left[(E - E_F)/k_BT\right]}. \tag{53}$$

By defining dimensionless variables $t_n = (E - E_{G,n}/2)/k_BT$ and $\eta_n = (E_F - E_{G,n}/2)/k_BT$, the integral in (53) is given by

$$\int_{E_{C,n}}^{\infty} \frac{1}{\sqrt{(E - E_{G,n}/2)}} \frac{dE}{1 + \exp\left[(E - E_F)/k_BT\right]} = \sqrt{k_BT} \int_0^{\infty} \frac{t_n^{-1/2}}{1 + \exp(t_n - \eta_n)}\, dt_n = \sqrt{k_BT}\Gamma(1/2)F_{-1/2}(\eta_n). \quad (54)$$

Γ represents the Gamma function, where $\Gamma(-1/2) = \sqrt{\pi}$, and $F_{-1/2}$ is the Fermi integral of order $-1/2$. The Fermi integral of type j is defined as

$$F_j(x) = \frac{1}{\Gamma(j+1)} \int_0^{\infty} \frac{t^j}{1 + \exp(t - x)}\, dt. \quad (55)$$

Finally, (53) can be written as

$$n = \sqrt{\frac{2k_BT}{\pi\hbar^2}} \sum_n \sqrt{m_n^*} F_{-1/2}(\eta_n). \quad (56)$$

REFERENCES

[1] *International Technology Roadmap for Semiconductors—2009 Edition*. [Online]. Available: http://public.itrs.net

[2] K. Novoselov, A. Geim, S. Morozov, D. Jiang, M. Katsnelson, I. Grigorieva, S. Dubonos, and A. Firsov, "Two-dimensional gas of massless Dirac fermions in graphene," *Nature (London)*, vol. 438, no. 7065, pp. 197–200, Nov. 2005.

[3] A. Geim and K. Novoselov, "The rise of graphene," *Nature Mater.*, vol. 6, no. 3, pp. 183–191, 2007.

[4] M. Lemme, T. Echtermeyer, M. Baus, and H. Kurz, "Towards graphene field effect transistors," *IEEE Electron Device Lett.*, vol. 28, no. 4, pp. 282–284, Apr. 2007.

[5] G.-C. Liang, N. Neophytou, D. Nikonov, and M. Lundstrom, "Performance projections for ballistic graphene nanoribbon field-effect transistors," *IEEE Trans. Electron Devices*, vol. 54, no. 4, pp. 677–682, Apr. 2007.

[6] T. Echtermeyer, M. Lemme, M. Baus, B. Szafranek, A. Geim, and H. Kurz, "Nonvolatile switching in graphene field-effect devices," *IEEE Electron Device Lett.*, vol. 29, no. 8, pp. 952–954, Aug. 2008.

[7] Z. Chen, Y. Lin, M. Rooks, and P. Avouris, "Graphene nano-ribbon electronics," *Phys. E*, vol. 40, no. 2, pp. 228–232, Dec. 2007.

[8] M. Han, B. Özyilmaz, Y. Zhang, and P. Kim, "Energy band-gap engineering of graphene nanoribbons," *Phys. Rev. Lett.*, vol. 98, no. 20, pp. 206805-1–206805-4, May 2007.

[9] X. Wang, Y. Ouyang, X. Li, H. Wang, J. Guo, and H. Dai, "Room-temperature all-semiconducting sub-10-nm graphene nanoribbon field-effect transistors," *Phys. Rev. Lett.*, vol. 100, no. 20, pp. 206803-1–206803-4, 2008.

[10] D. Areshkin, D. Gunlycke, and C. White, "Ballistic transport in graphene nanostrips in the presence of disorder: Importance of edge effects," *Nano Lett.*, vol. 7, no. 1, pp. 204–210, Jan. 2007.

[11] D. Gunlycke, D. Areshkin, and C. White, "Semiconducting graphene nanostrips with edge disorder," *Appl. Phys. Lett.*, vol. 90, no. 14, pp. 142104-1–142104-3, Apr. 2007.

[12] Y. Yang and R. Murali, "Impact of size effect on graphene nanoribbon transport," *IEEE Electron Device Lett.*, vol. 31, no. 3, pp. 237–239, Mar. 2010.

[13] M. Evaldsson, I. V. Zozoulenko, H. Xu, and T. Heinzel, "Edge-disorder-induced anderson localization and conduction gap in graphene nanoribbons," *Phys. Rev. B, Condens. Matter*, vol. 78, no. 16, pp. 161407(R)-1–161407(R)-4, Oct. 2008.

[14] T. C. Li and S. P. Lu, "Quantum conductance of graphene nanoribbons with edge defects," *Phys. Rev. B, Condens. Matter*, vol. 77, no. 8, pp. 085408-1–085408-8, Feb. 2008.

[15] A. Cresti and S. Roche, "Range and correlation effects in the edge disordered graphene nanoribbons," *New J. Phys.*, vol. 11, no. 9, pp. 095004-1–095004-12, Sep. 2009.

[16] G. Fiori and G. Iannaccone, "Simulation of graphene nanoribbon field-effect transistors," *IEEE Electron Device Lett.*, vol. 28, no. 8, pp. 760–762, Aug. 2007.

[17] A. Lherbier, B. Biel, Y. Niquet, and S. Roche, "Transport length scales in disordered graphene based materials: Strong localization regime and dimensionality effects," *Phys. Rev. Lett.*, vol. 100, no. 3, pp. 036803-1–036803-4, Jan. 2008.

[18] E. R. Mucciolo, A. H. C. Neto, and C. H. Lewenkopf, "Conductance quantization and transport gaps in disordered graphene nanoribbons," *Phys. Rev. B, Condens. Matter*, vol. 79, no. 7, pp. 075407-1–075407-3, Feb. 2009.

[19] Y. Yoon and J. Guo, "Effect of edge roughness in graphene nanoribbon transistors," *Appl. Phys. Lett.*, vol. 91, no. 7, pp. 073103-1–073103-3, Aug. 2007.

[20] S. Dubois, A. Lopez-Bezanilla, A. Cresti, F. Triozon, B. Biel, J. Charlier, and S. Roche, "Quantum transport in graphene nanoribbons: Effects of edge reconstruction and chemical reactivity," *ACS Nano*, vol. 4, no. 4, pp. 1971–1976, Apr. 2010.

[21] D. Gunlycke and C. T. White, "Scaling of the localization length in armchair-edge graphene nanoribbons," *Phys. Rev. B, Condens. Matter*, vol. 81, no. 7, pp. 075434-1–075434-6, Feb. 2010.

[22] D. Gunlycke and C. T. White, "Tight-binding energy descriptions of armchair-edge graphene nanostrips," *Phys. Rev. B, Condens. Matter*, vol. 77, no. 11, pp. 115116-1–115116-6, Mar. 2008.

[23] S. M. Goodnick, D. K. Ferry, C. W. Wilmsen, Z. Liliental, D. Fathy, and O. L. Krivanek, "Surface roughness at the Si(100)- SiO_2 interface," *Phys. Rev. B, Condens. Matter*, vol. 33, no. 12, pp. 8171–8186, Dec. 1985.

[24] T. Fang, A. Konar, H. Xingi, and D. Jena, "Mobility in semiconducting graphene nanoribbons: Phonon, impurity, and edge roughness scattering," *Phys. Rev. B, Condens. Matter*, vol. 78, no. 20, pp. 205403-1–205403-8, Nov. 2008.

[25] S. Datta, *Electronic Transport in Mesoscopic Systems*. New York: Cambridge Univ. Press, 1995.

[26] J.-H. Chen, C. Jang, S. Xiao, M. Ishighami, and M. Fuhrer, "Intrinsic and extrinsic performance limits of graphene devices on SiO_2," *Nature Nanotechnol.*, vol. 3, no. 4, pp. 206–209, Apr. 2008.

[27] A. Akturk and N. Goldsman, "Electron transport and full-band electron-phonon interactions in graphene," *J. Appl. Phys.*, vol. 103, no. 5, pp. 053702-1–053702-8, Mar. 2008.

[28] D. A. Abanin, S. V. Morozov, L. A. Ponomarenko, R. V. Gorbachev, A. S. Mayorov, M. I. Katsnelson, K. Watanabe, T. Taniguchi, K. S. Novoselov, L. S. Levitov, and A. K. Geim, "Giant nonlocality near the Dirac point in graphene," *Science*, vol. 332, no. 6027, pp. 328–330, Apr. 2011.

[29] N. Castro and H. Antonio, "Another spin on graphene," *Science*, vol. 332, no. 6027, pp. 315–316, Apr. 2011.

[30] G. Xu, C. M. Torres, Jr., J. Tang, J. Bai, E. B. Song, Y. Huang, X. Duan, Y. Zhang, and K. L. Wang, "Edge effect on resistance scaling rules in graphene nanostructures," *Nano Lett.*, vol. 11, no. 3, pp. 1082–1086, Mar. 2011.

[31] F. Flores, B. Biel, A. Rubio, F. J. Garcia-Vidal, C. Gomez-Navarro, P. de Pablo, and J. Gomez-Herrero, "Anderson localization regime in carbon nanotubes: Size dependent properties," *J. Phys., Condens. Matter*, vol. 20, no. 30, pp. 304211-1–304211-7, Jul. 2008.

[32] D. J. Thouless, "Localization distance and mean free path in one-dimensional disordered systems," *J. Phys. C, Solid State Phys.*, vol. 6, pp. 49–51, Feb. 1973.

Arash Yazdanpanah Goharrizi received the B.S. degree in electronics from the Shahid Bahonar University of Kerman, Kerman, Iran, in 2000, the first M.S. degree in power systems in 2004, and the second M.S. degree in electronics from the Tabriz University, Tabriz, Iran, in 2005. He is currently working toward the Ph.D. degree in nanoelectronics at the University of Tehran, Tehran, Iran.

From 2005 to 2007, he was a Design Engineer with the National Iranian Copper Industries Company. He is also currently with the Institute for Microelectronics, Technische Universität Wien, Wien, Austria. His research topics are voltage stability in power networks, fiber Bragg gratings in optical applications, semiconductor devices, and quantum transport in nanostructures.

Mahdi Pourfath (M'08) was born in Tehran, Iran, in 1978. He received the B.S. and M.S. degrees in electrical engineering from Sharif University of Technology, Tehran, in 2000 and 2002, respectively, and the Ph.D. degree in technical sciences from Technische Universität Wien, Wien, Austria, in 2007.

Since October 2003, he has been with the Institute for Microelectronics, Technische Universität Wien. He is also currently with the Department of Electrical and Computer Engineering, University of Tehran, Tehran. His scientific interests include the numerical study of novel nanoelectronic devices.

Morteza Fathipour (M'90) received the M.S. and Ph.D. degrees in solid-state electronics from Colorado State University, Fort Collins, in 1980 and 1984, respectively.

From 1984 to 1986, he taught at Sharif University of Technology, Tehran, Iran. He then joined the Department of Electrical and Computer Engineering, University of Tehran, Tehran, where he is the Founder of the Technology in Computer-Aided Design Laboratory. His research interests include device physics, semiconductor interface, process/device design, simulation, modeling and characterization for ultralarge-scale integration devices, computer-aided design development for process and device design, fabrication of nanodevices, and optoelectronics.

Hans Kosina (S'89–M'93) received the "Diplomingenieur" degree in electrical engineering and the Ph.D. degree from the Technische Universität Wien, Wien, Austria, in 1987 and 1992, respectively, and the "venia docendi" in microelectronics from Technische Universität Wien, Wien, Austria, in 1998.

For one year, he was with the Institute of Flexible Automation, Technische Universität Wien, and then joined the Institute for Microelectronics, Technische Universität Wien, where he is currently an Associate Professor. In summer of 1993, he was a Visiting Scientist at Motorola Inc., Austin, TX, and in summer of 1999, a Visiting Faculty at Intel Corporation, Santa Clara, CA. His current research interests include device modeling of semiconductor devices, nanoelectronic devices, organic semiconductors and optoelectronic devices, development of novel Monte Carlo algorithms for classical and quantum transport problems, and computer-aided engineering in ultralarge-scale integration technology.

Siegfried Selberherr (M'79–SM'84–F'93) was born in Klosterneuburg, Austria, in 1955. He received the Diplomingenieur degree in electrical engineering and the Ph.D. degree in technical sciences from the Technische Universität Wien, Wien, Austria, in 1978 and 1981, respectively.

He has been holding the venia docendi on computer-aided design since 1984. Since 1988, he has been the Chair Professor of the Institut für Mikroelektronik, Technische Universität Wien. From 1998 to 2005, he served as the Dean of the Fakultät für Elektrotechnik und Informationstechnik. He has published more than 250 papers in journals and books, where more than 80 appeared in IEEE TRANSACTIONS. He and his research teams achieved more than 750 articles in conference proceedings, of which more than 100 have been with an invited talk. He authored two books and coedited 25 volumes, and so far, he has supervised more than 90 dissertations. His current research interests are modeling and simulation of problems for microelectronics engineering.